Nanoscale

Accepted Manuscript

This article can be cited before page numbers have been issued, to do this please use: D. Qi, S. Tang, L. Wang, S. Dai, X. Shen, C. Wang and S. Chen, *Nanoscale*, 2018, DOI: 10.1039/C8NR00210J.

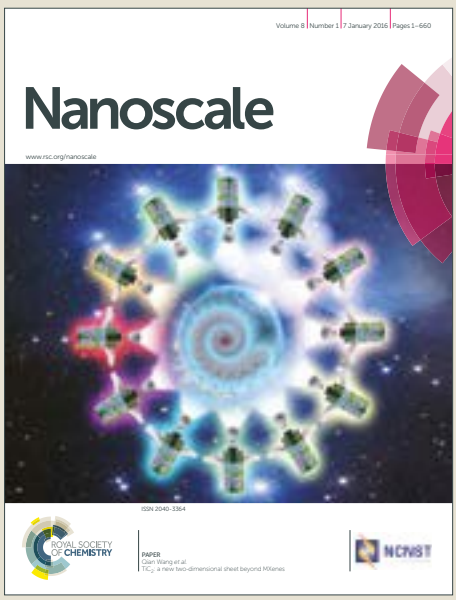

View Article Online
DOI: 10.1039/C8NR00210J

Nanoscale

ARTICLE

Pulse Laser Induced Size-controllable and Symmetrical Ordering of Single Crystal Si Islands

Received 00th January 20xx,
Accepted 00th January 20xx

DOI: 10.1039/x0xx00000x

www.rsc.org/

Dongfeng Qi,[*a b c] Shiwei Tang[a] Letian Wang[b] Shixun Dai[a] Xiang Shen[a] Chen Wang[d] and Songyan Chen[c]

Optically electric and magnetic resonances induced dielectric nanostructures have drawn significant attention due to their future applications of tunable electronic and optoelectronic device. In this letter, we describe an ultrafast and large-area method to construct symmetrical and single crystal Si island structures directly on Si substrate by pulse laser dewetting method. The tunable surface electric field intensity distribution can convert the stochastic dewetting process into a deterministic one (classical dipole mode and Mie resonance dipole mode) on the predefined Si pit arrays via laser dewetting method. In this condition, these pre-patterned Si substrate structures not only induce high spatial ordering of islands but also improve their size uniformity. By adjusting the laser fluence, the diameter of the signal crystal Si islands can be selected in the range of 41.7 nm to 147.1 nm.

Introduction

There has been a keen interest in Si-based island nano-structures, motivated by future applications to tunable electronic and optoelectronic devices, and a variety of methods have been proposed to fabricate these structures [1-4]. In particular, silicon island structures have been studied as new materials to achieve photonic crystals, solar cells, sensors, and thermoelectric devices due to the tunable band-gap, the electric dipole resonance peaks located in the visible and near-infrared range [5-10], and the abundance and implicit compatibility with current semiconductor processing technologies [11].

As well known to all, tuning and programming of the surface nanostructures geometrical features and photonic properties are widely used in structural color, optical data storage, and active nanophotonic devices [12-14]. Differently from the former low aspect ratio islands (pyramid, dome, barn and cupola), three dimensions of the size of the high aspect ratio islands, and the movement of electrons in the islands is subject to limitations, and quantum-confined in three of their dimensions. With tailoring the band structure artificially with uniformly shaped islands and the three-quantum confinement effect, combined with modulated-doping and carrier filling effect, high efficiency light-emitting Si-based nano-structures are expected, which could be beneficial for the monolithic integration of Si-based photonic devices [15-16]. In addition to disorder surface nanostructures, symmetrical island structures should offer not only further tunability and engineering capabilities of the enhanced electric and magnetic fields but it should also reveal the physics of hotspots and near-field distributions known to be very important for islands oligomers with Fano-type resonances, strong inter-particle interactions [17-21]. Fano-type resonances arise directly from the coherent coupling and interference of bright and dark plasmon modes, which can be used for potential biological labeling and diagnostic applications [22-27]. Recently, there are some references have reported that the periodic patterned structures on metallic surface, such as pit and pillar arrays, can modify the electric intensity distribution of the incident laser, which can induce surface plasmon modes, and this field distribution always shows the presence of dipole or quadrupole mode and suggests that large field enhancements appear at the tips of these surface patterned structures. Besides, symmetrical island structures will shed light into building more complex nanostructures, as nanoparticles are the most basic nano building-blocks widely used functional components for a broad range of future applications, from chemical sensing to energy storage to active nanophotonic devices [28-29].

Since, Some other groups have reported that surface nanoisland structures can be fabricated by various top-down and bottom-up fabrication methods [30-32]. However, the top-down method is usually associated with high-cost, reactive ion etching, e-beam lithography and spontaneous self-assembly represent two extremes in nano-manufacturing [33]. On the other hand, the Si-based nanostructures fabricated by the

a. Laboratory of Infrared Materials and Devices, The Research Institute of Advanced Technologies, Ningbo University, Ningbo, Zhejiang, 315211, People's Republic of China.
b. Laser Thermal Laboratory, Department of Mechanical Engineering, University of California, Berkeley, Berkeley, CA 94720-1740, USA.
c. Department of Physics, Xiamen University, Xiamen, 361005, People's Republic of China
d. School of Optoelectronic and Communication Engineering, Xiamen University of Technology, Xiamen, Fujian 361024, China

*Corresponding author. Ningbo University, Ningbo, Zhejiang, 315211, China. E-mail: qidongfeng@nbu.edu.cn

Electronic Supplementary Information (ESI) available: [details of any supplementary information available should be included here]. See DOI: 10.1039/x0xx00000x

View Article Online
DOI: 10.1039/C8NR00210J

bottom up vapor–liquid–solid (VLS) method inevitably contain saturated dopants from the metal catalyst. As is well-known to all, metal impurities in photoelectric devices show serious problems of low yields and poor performances of devices due to induced detrimental effects, for example, noble metal impurities will form deep level centers, which ultimately act as efficient generation recombination centers to increase the leakage current of junctions [34-35]. Recently, micro/nanostructure patterning with an ultra-short pulse laser source is regarded as a unique technique, which can modify the surface morphology of the materials with tunable and high efficiency, and it has attached great research interests in the fields of laser processing, solar cells, optical memories and optoelectronics [36-38]. On the other hand, pattern-guided laser and thermal dewetting, as well as liquid-assembly, can produce periodic metallic and dielectric nanostructures with a good combination of fidelity and low cost [39-40]. Therefore, both pattern and tune the particle number, placement, and size should be developed, and the availability of optically reconfigurable nanophotonics that are based on Si-based materials, suggests that a low-cost optically tunable approach is also needed for silicon based photonics and structural color. In this condition, a deeper exploration of relevant mechanism is needed to achieve a direct and clear relationship between laser irradiation conditions and the induced nanostructures, for a better control to fabricate desired nanostructure for practical applications, which have both some advantages in nanofabrication and photoelectric application.

Experimental

In order to experimentally observe the discussed field enhancement effort, patterned silicon pits are firstly fabricated using a standard top-down nanofabrication approach in this work. What is more import is that we can also obtain the experimental demonstration of electric hotspots of silicon nanopit arrays after pluse laser irradiation, which directly results in the symmetrical ordering of single crystal Si islands on pre-patterned Si substrate. Si pit arrays fabrication via nano-imprint stamp procedure employed in this paper is illustrated in figure 1(a). The thermal resist layer containing a periodic array of deep circular pits, 250 nm in diameter, 350 nm in height, and 500 nm in periodicity, are formed on the 4 inch Si substrate，as shown in figure 1(a), and the morphology of the patterned thermal resist layer is shown in the supporting file, figure S1. After the surface is cleaned, the sample is etched by reactive ion etching technology (RIE), further, the structural parameters of the array could be tuned and controlled only by changing the etching time but keeping the other conditions unchanged, the detail of the process is listed in the in the supporting file. SEM images in figure 1(b) demonstrate the arrays with different disks' diameters from 150 to 250 nm after etching for different etching times (15 s and 20 s). Obviously, most of the Si nanodisks formed by the reactive ion etching are uniform in size and in shape, and the sample size is 2×2 cm. Next, the prepared patterned Si samples are processed by the pulse laser to incur some discussed electric hotspots, and peridoic Si island structures directly appear on the Si pit arrays substrate, as shown in figure 1(c). Basing on the different size and shape of pit arrays, axial or tetragonal symmetric Si islands can be located around each pit. In this work, the schematic illustration of the laser processing system is shown in figure S2. A linear polarization KrF excimer laser of 248 nm wavelength and 25 ns temporal width impinges on Si substrate targets. The laser beam is focused by a 5× infinity corrected, non-achromatic long working distance objective lens at normal incidence. The white light is employed as an illumination source to provide temporally resolved images, and these images are captured by a charge coupled device (CCD) camera. The oscilloscope is used to record the actual duration time of the processing laser signal. To ensure true representation, at least four samples are examined for each laser fluence.

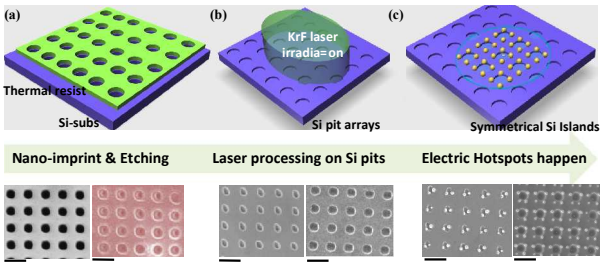

Figure 1. Scheme of the fabrication procedures of symmetrical islands on Si pit arrays. (a):Thermal resist layer is spin-coated on the Si surface and intermediate polymer sheet with circular post patterns is used as a mask to fabricate circular pit arrays on Si substrate. (b): Removal of thermal resist and Si wafer is subsequently etched to be a pit template with different size pits. (c): Nanosecond laser dewetting process and electric hotspots happen. The scale bars in SEM images are all 500 nm.

The morphologies of the formed surface structures were characterized by a scanning electron microscopy system (SEM, LEO 1530, with an operating voltage of 20 kV). The depth and diameter of the naoholes can be analyzed by atomic force microscopy (AFM) using Seiku Instruments SPI4000/SPA-400 system operating in tapping mode.

Results and discussion

To further description the modification of the symmetrical island structures on Si pit arrays, we depict distinct stages of the periodic island structures modification process and the corresponding dewetting process in figure 2. As demonstrated in figure 2, we show the scanning electron microscopy (SEM) images of Si films with increasing of laser fluence, which directly depicts the general effects of patterned Si on the morphological evolution. SEM images in the first line show morphologies of unpatterned Si substrate after different laser fluences irradiation. Firstly, disordered single crystal Si islands morphology can be induced on the surface after 400 mJ/cm^2 laser irradiation, as shown in figure 3(a). The inset image of figure 3(a) is the selected area electron diffraction (SAED) pattern of the island, whereas the SAED pattern confirms the

View Article Online
DOI: 10.1039/C8NR00210J

[100]-growth direction of the island, which is in accordance with the Si substrate. What more imporant is that we can obtain Si islands with different diameters and densities via changing the laser fluence of the incident laser, as shown in figure 2(Si substrate sample). In figure 3 (b), with increasing of laser fluences, the diameter of the laser-induced Si island becomes larger from 41.7 nm to 147.1 nm, oppositely, the density of these random islands decrease from 1.1e^{9} to 2.8e^{10}. The testing method is shown in the supporting information, figure S4 and figure S5. For these patterned Si substrates, surface morphologies are measured by Scanning Electron Microscopy (SEM), and these images are listed in the second and third lines. For the elliptic pit arrays, the short axis of each pits is of 150 nm diameters with long axis of about 230 nm. Most interestingly, after laser irradiation, the surface islands are located at the edge of each pit, which align in a symmetrical pattern along the short axis of the pits. Besides, the diameter of these islands grows larger and dual-islands forms as the increasing of the laser fluence, signifying these nearby small size islands aggregation to bigger islands at higher laser fluence (450 mJ/cm^2). Similar dewetting behaviour of islands around the edge of the pits are also observed for samples with larger diameter circle pits. Perfect circle pit arrays can be formed after 20 s RIE etching, and the pits are of 225 nm diameters with a spacing of about 275 nm. After laser irradiation, symmetrical islands can be aligned in a circular fashion on the four corners of the surface pits, which also grow larger as the increasing of the laser fluence. Basing on the surface pit arrays, the melted islands at preferential site can be achieved. However, if the laser fluence exceeds the optimum level (above 550 mJ/cm^2), the surface disordered island morphology takes place symmetrical islands morphology, and these surface pit arrays also disappear, in figure 2, which is mainly attributed to the stress-induced compression effect caused by thermal expansion of solid and liquid materials at higher laser fluence [42-46].

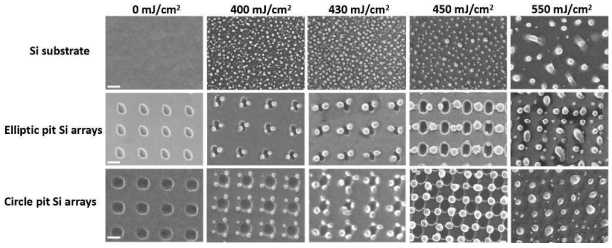

Figure 2. SEM of Si surface pit arrays and the corresponding circularly ordered Si islands in patterned region after nanosecond pulse laser irradiation at different fluences. The fluence is increased from left to right (the center of beam), and the scale bars in SEM images are all 200 nm.

From above analyses, we can fabricate Si islands with controllable diameter and preferential site at certain laser fluence. To further confirm the subsurface melting mechanism leading to the islands formation, we have studied their thermodynamic process. From the heat flow calculation, several parameters such as the depth of the molten layer, the melting duration and surface temperature of the samples can be evaluated as a function of laser fluence, and the detail information is shown in supporting file. Figure S 3(a) and (b) show the sample surface temperatures vs. time and maximum temperature vs. depth at various laser energy densities from 400 to 550 mJ/cm^2, respectively. The melting temperature threshold (melt point) for Si is marked with horizontal dash line. When irradiating Si with pulse laser at a sufficient fluence (above 400 mJ/cm^2), a melted zone is formed on the surface. As the laser fluence is high enough, the melted zone is well defined and a sharp transition between the liquid and solid phase is formed, and the surface island structures can be formed by the full melting phenomenon [30-33].

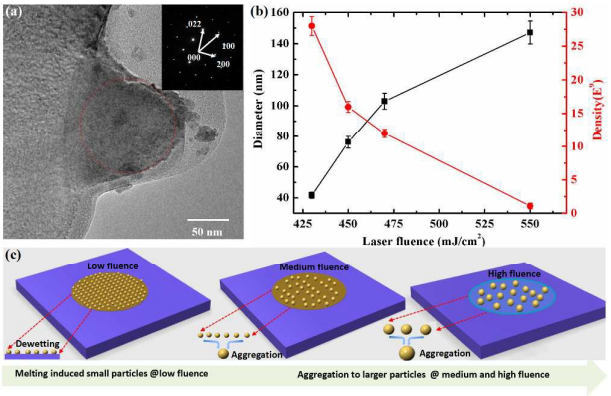

Figure 3. (a) TEM images of the island structures (with mean diameters of 80 nm); the inset image is the corresponding selected area electron diffraction image (which shows the single crystalline of the Si island). Laser fluence: 450 mJ/cm^2. (b) The mean diameters, and the island density of Si islands with different laser fluence: 430 mJ/cm^2, 450 mJ/cm^2, 480 mJ/cm^2 and 550 mJ/cm^2, respectively. The mean diameters, in nanometers (nm) and the density (cm^{-2}), are (41.7, 2.8e^{10}), (78.6, 1.6e^{10}), (102.9, 1.2e^{10}) and (147.1, 1.1e^{9}), respectively. (c) Give a schematic illustration of mechanisms responsible for nanosecond laser-induced formation of Si islands on flat Si substrate, small island structures can be formed by fully melting phenomenon at lower fluence in the spot center, and aggregation to bigger sized islands at higher fluence.

The melted depth and melting duration at various laser fluences are extracted and plotted in figure S3(c). The melting duration time of the surface and melted depth increase with laser fluence in the range of 400 to 550 mJ/cm^2. Incident laser with higher fluence can induce a longer dewetting duration time and the larger dewetting depth, as shown in figure S3(c), which can supply significant energy transfer and signify small islands aggregation to bigger sized islands. It is worth noting that island morphology is formed after laser irradiation, and as the fluence increases, the size of island structures increases

View Article Online
DOI: 10.1039/C8NR00210J

while the density decrease, respectively, implying melting phenomenon happens. In conclusion, if the laser intensity in the spot center is below the ablation threshold, the nanosecond laser pulse causes local dewetting of the untreated Si layer in the spot center. In this case, disordered island structures can be formed by fully melting phenomenon after laser irradiation, wherein the larger islands scavenge smaller ones, broadening the size distribution in the dewetting area after higher laser fluence for all samples, as shown in figure 3(c).

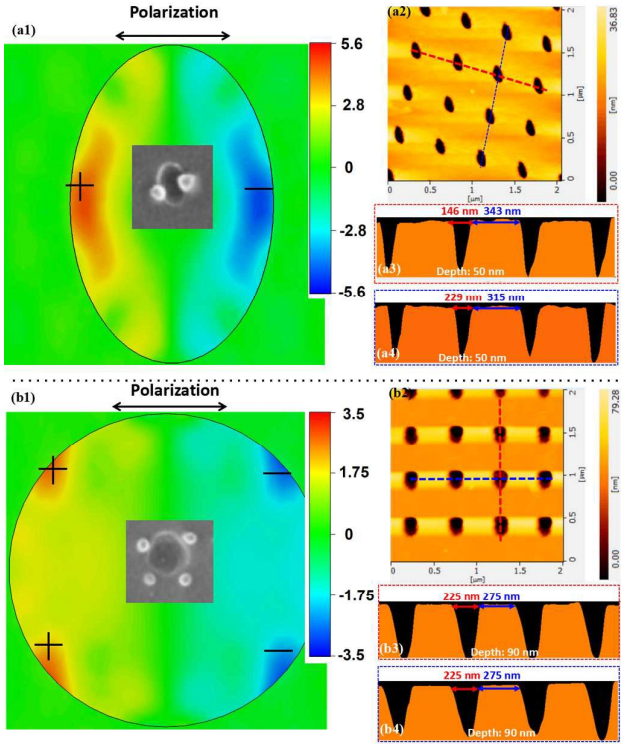

Figure 4. (a1, b1) are calculated electric field intensities ($|E|^2$) distribution of patterned Si pit under a 248 nm incident laser irradiation, which are calculated by FDTD method, and the insert images are the corresponding SEM images, respectively; (a2, b2), (a3, b3) and (a4, b4) are AFM images of height scans Si nanowell with different sizes.

In order to clearly indentify the symmetrical properties of laser-induced islands from the Si surface pit arrays, the local electric field distributions of patterned Si at 248 nm (Figure 4) are calculated by finite-difference time-domain (FDTD) method, and all parametes of the pits, calculated in this software, are all obtained from AFM images, as shown in figure S6. During the calculation, the excitation laser beam was set as a plane wave and vertically incident upon the pre-patterned Si substrate structures, and the detail information is listed in supporting file. It is also noted that the calculated near-field enhancement of these two modes corresponds well to the experimental results shown in Figure 4 (a1, b1). For the elliptic pit arrays, in figure 4(a1), under perpendicular incidence irradiation, only the dipole mode was excited for such elliptic Si surface pit arrays at the wavelength of 248 nm, and field maximum points are located at the center of the side edges after laser irradiation. This field distribution shows the presence of classical dipole mode and suggests that large field enhancements appear at the edge of each elliptic pit [47-48]. For the circle pit arrays, in figure 4(b1), four field maximum points along the four side edges can be seen, which implies the existence of Mie resonance dipole mode. And the absorption spectrum for the pit are shown in figure S7. The absorption spectrum of the elliptic pit and circle pit result shows the resonance at around 248 nm, and the Q factor (Intensity/FWHM) are 414 and 292, respectively. Some references have reported that a control over the position, number and relative orientation of Mie resonance can be obtained by modifying the size, shape and orientation of the milled patterns [37-39]. For example, patterned cylinders (diameter: 350 nm) can exhibit a broadband surface resonance for an input wavelength of approximately 248 nm pulse laser, which the cylinders can be treated as oblate spheroids with a large depolarization factor along the revolution axis and they behave like circular patch nanoantennas [49]. And pulse laser treating the triangle and square patterned metallic thin films has been studied as a means to direct the assembly of thin film materials. Besides, some investigations highlight the versatility of this approach since the fabrication of individual or assemblies of Mie resonators are produced by tuning the dewetting speed, the silicon thickness, the pattern size and symmetry as well as the milling of local defects acting as nucleation centers for the island growth [49-51]. Further to the pre-patterned substrate, where temperature of the dipole or Mie resonators areas is above the melting threshold, complete melting and damage to the certain areas can happen.

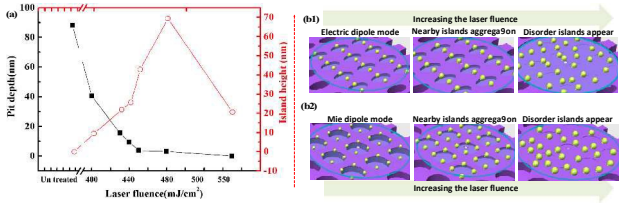

Figure 5. (a) The summary of the tendency of depth of Si pit substrate and height of Si islands vs laser fluence. (b1, b2) Give a schematic illustration of mechanisms responsible for nanosecond laser-induced formation of surface ordered Si islands in patterned region.

View Article Online
DOI: 10.1039/C8NR00210J

Our fabrication approach of symmetrical ordering Si islands is strongly versatile, as it can be applied not only to produce high-densities of dipole or Mie resonators with high or low ordering, but also to create single-crystalline Si island structures whose number and position can be tuned when the dewetting process is assisted by the pre-patterned Si substrate. The patterned edges act as programmable instabilities and, when laser heated, assemble in predictable ways. The distribution of the surface ordered Si islands is correlated to the additional dipole or Mie resonators on the pre-patterned substrate. To further describe the modification of the symmetrical island structures on Si pit arrays we depict distinct stages of the periodic island structures modification process and the corresponding dewetting processing in figure 5(b1, b2). At lower laser fluence, the space between the pits is small and the melting depth is large enough, it allows for material exchange among islands and migration toward the pit edges. Hence, basing on the surface dipole mode and Mie resonance dipole mode, dewetting phenomenon takes place around the pit edges, and dewetting phenomenon can be confined at the edge of the pit, which lead to the formation of symmetrical islands on the certain position of the pits [47-48, 52]. With the increasing of laser fluence, the surface pits can supply significant mass transfer and larger symmetrical islands are formed at higher laser fluence, which results in the depth of these surface holes decreasing and size of islands increasing, as shown in figure 5 (a), the data in Figure 5a are from Figure S8 in supporting information, we select circle pits for example. If the laser fluence exceeds the certain threshold of each sample (above 550 mJ/cm^2 in this experiment), the SEM images of patterned Si samples show that symmetrical islands are replaced by disorder island structures on the surface. As the pulse laser fluence is high enough, the melted zone is well defined and a sharp transition between the liquid and solid phase is formed on the edge, inducing a longer dewetting duration time and the larger dewetting depth (above 200 nm), as calculated in figure 3(b, c). In this case, the dewetting depth is much larger than that of depth of these holes, resulting the disappearance of these surface pits and the formation of disorder island structures, in figure S8, S9. This result demonstrates that we can selectively excite classical dipole mode with two hotspots and Mie resonance dipole mode with four hotspots by manipulating the size and shape of the surface pits, which can induce deterministic Si islands structures on the Si substrate.

Conclusions

In conclusion, the pre-patterned Si pit array substrate film can be dewetted into symmetrical and single crystal Si island structures array upon KrF excimer nanosecond laser irradiation. The patterned pit arrays can induce the local electric field distributions when 248 nm pulse laser irradiation, resulting in the field maximum points are located at the certain position of the pit side edges. These field distributions show the presence of classical dipole mode and Mie resonance dipole mode by adjusting the shape of the surface pit arrays. In this condition, symmetrical Si island structures can be formed on these surface electric hotspots by laser-induced directed dewetting processing.

Conflicts of interest

There are no conflicts to declare.

Acknowledgements

This work was supported by the National Natural Science Foundation of China under Grant number 61705117, 61534005, 61534005 and 61474081, and the Key Research and Development Program of Zhejiang Province (2017C01005). It is also sponsored by K. C. Wong Magna Fund in Ningbo University.

Notes and references

1 Y. Cui. C. M. Lieber, *Science,* 2001**, 291**, 851.
2 V. Schmidt, H. Riel, S. Senz, S. Karg, W. Riess, U. G¨osele, *Small,* 2006, **2**, 85–88.
3 B. Tian, X. Zheng, T. J. Kempa, Y. Fang, N. Yu, G. Yu, J. Huang, C. M. Lieber, *Nature,* 2007**, 449**, 885–890.
4 F. Patolsky, G. Zheng, C. M. Lieber, *Nat. Protoc.,* 2006, **1**, 1711–1724.
5 W. Porod, C. S. Lent, G. H. Bernstein, A. O. Orlov, I. Amlani, G. L. Snider, J. Merz, L. *Int. J. Electron.* 1999, **86**, 549.
6 S. S. Li, G.Long, F. S. Bai, S. L. Feng, H. Z. Zheng, *Proc. Natl. Acad. Sci. U. S. A*. 2001, **98**, 11847.
7 G. Burkard, D. Loss, D. P. DiVincenzo, *Phys. Rev. B: Condens. Matter Mater. Phys.* 1999, **59**, 2070.
8 O. Leifeld, A. E. Muller, D. Grutzmacher, K. Kern, *Thin Solid Films,* 2000, **380**, 176.
9 J. Y. Kim, S. H. Ihm, J, H. Seok, C. H. Lee, E. K. Suhand, H. J. Lee, *Thin Solid Films,* 2000, **369**, 96.
10 Y. Wakayama, G. Gerth, P. Werne, L. V. Sokolov, *Surf. Sci.* 2001, **493**, 399.
11 V. I. Klimov, A. A. Mikhailovsky, S. Xu, A. Malko, J. A. Hollingsworth, C. A. Leatherdale, H. J. Eisler, M. G. Bawendi, *Science,* 2000, **290**, 314.
12 X. Zhu, W. Yan, U. Levy, N. A. Mortensen, A. Kristensen, *Sci. Adv.,* 2017, **3**(5), e1602487.
13 M. Wuttig, N. Yamada, *Nat. Mater.* 2007, **6**, 824–832.
14 Q. Wang, E. T. F. Rogers, B. Gholipour, C.-M. Wang, G. Yuan, J. Teng, N. I. Zheludev, *Nat. Photonics,* 2016, **10**, 60– 65.
15 X. G. Peng, L. Manna, W. D. Yang, J. Wickham, E. Scher, A. Kadavanich and A. P. Alivisatos, Nature, 2000, **404**, 59.
16 V. I. Klimov, A. A. Mikhailovsky, S. Xu, A. Malko, J. A. Hollingsworth, C. A. Leatherdale, H.-J. Eisler and M. G. Bawendi, Science, 2000, **290**, 314.
17 U. Zywietz, A. B. Evlyukhin, C. Reinhardt, B. N. Chichkov, *Nat. Commun.,* 2014**, 5**, 3402.
18 J. H. Yoo, J. B. In, C. Zheng, I. Sakellari, R. N. Raman, M. J. Matthews, S. Elhadj, C. P. Grigoropoulos, *Nanotechnology* 2015**, 26**, 165303.
19 Y. H. Fu, Y. H. A. I. Kuznetsov, A. E. Miroshnichenko, Y. F. Yu, B. Luk'yanchuk, *Nat. Commun*., 2013, **4**, 1527.
20 S. Person, M. Jain, Z. Lapin, J. J. Saénz, G. Wicks, L. Novotny, *Nano Lett*. 2013, **13**, 1806−1809.

View Article Online
DOI: 10.1039/C8NR00210J

21 B. Rolly, B. Stout, N. Bonod, *Opt. Express,* 2012, **20**, 20376–20386.
22 J. Q. Li, N. Verellen, D. Vercruysse, T. Bearda, L. Lagae, P. V. Dorpe, *Nano. Lett.* DOI: 10.1021/acs.nanolett.6b01519.
23 Z. X. Li, Y. Yu, Z. Y. Chen, T. R. Liu, Z. K. Zhou, J. B. Han, J. T. Li, C. J. Jin, X. H. Wang, *J. Phys. Chem. C.,* 2013, **117**, 20127–20132.
24 Y. Y. Tanaka, T. Shimura, *Nano Lett.* 2017, **17**, 3165–3170.
25 Q. Sun, H. Yu, K. Ueno, A. Kubo, Y. Matsuo, H. Misawa, H. *ACS Nano,* 2016, **10**, 3835–3842.
26 W. Cao, R. J. Singh, I. A. I Al-Naib, M. X. He, A. J. Taylor, and W. L. Zhang, *Optic Lett.*, 2012, **37**(16), 3366.
27 J. J. Mock, D. R. Smith, and S.Schultz*, Nano Lett.*, 2003, **3**(4), 485-491.
28 S. X. Lin, C. Y. Wong, E. Y. B. Pun, F. Song, *Nanotechnology* 2010, **21** (5), 055203.
29 S. Kawata, Y. Inouye, P. Verma, *Nat. Photonics* 2009, **3** (7), 388–394.
30 R. R. He, R. Fan, A. I. Hochbaum, C. Carraro, R. Maboudian and P. D. Yang, *Adv. Mater.*, 2005, **17**, 2098.
31 Y. Y. Wu and P. D. Yang, *J. Am. Chem. Soc.*, 2001, **123**, 3165.
32 H.F.Yan,Y.J.Xing,Q.L.Hang,D.P.Yu,Y.P.Wang,J.Xu, Z. H. Xi and S. Q. Feng, Chem. Phys. Lett., 2000, **323**, 224.
33 D. F. Qi, H. H. Liu, W. Gao, Q. Q. Sun, S. Y. Chen, W. Huang, C. Li, H. K.Lai, *J. Mater. Chem. C.* 2013, **1**, 6878.
34 K. Q. Peng, A. J. Lu, R. Q. Zhang and S. T. Lee, *Adv. Funct. Mater.*, 2008, 18, 3026–3035.
35 P. Gorostiza, R. Diaz, J. Servat, F. Sanz and J. R. Morante, *J. Electrochem. Soc.*, 1997, **144**, 909.
36 S. Hong, H. Lee, J. Yeo, S. H. Ko, *Nano Today,* 2016, **11**, 547–564.
37 M. Sygletou, C Petridis, E. Kymakis, E. Stratakis, *Adv. Mater.,* 2017, **29**, 1700335.
38 S. V. Makarov, A. S. Zalogina, M. Tajik, D. A. Zuev, M. V. Rybin, A. A. Kuchmizhak, S. Juodkazis, Y. Kivshar, *Laser Photonics Rev.,* 2017, **11**, 1700108.
39 H. Wu, G. Chan, J. W. Choi, I. Ryu, Y. Yao, M. T. McDowell, S. W. Lee, A. Jackson, Y. Yang, L. Hu, Y. Cui, *Nat. Nanotechnol.,* 2012, **7**, 310– 315。
40 J. D. Fowlkes, N. A. Roberts, Y. Wu, J. A. Diez, A. G. González, C.Hartnett, K. Mahady, S. Afkhami, L. Kondic, P. D. Rack, *Nano Lett.,* 2014, **14**, 774– 782
41 M. G. Rahimian, F. Bouchard, H. Al-Khazraji, E. Karimi, P. B. Corkum, and V. R. Bhardwaj, *APL Photonics.,* 2017, **2**, 086104.
42 D. F. Qi, D. P. Paeng, J. Y. Yeo, E. Kim, L. T. Wang, S. Y. Chen, and C. P. Grigoropoulos, *Appl. Phys. Lett.,* 2016, **108**, 211602.
43 B. K. Nayak, K. Sun, C. Rothenbach, and M. C. Gupta, *Applied optics,* 2011, **50** (16), 2349-2355.
44 M. Kawasaki, and M, Hori, *J. Phys. Chem. B* 2003, ***107,*** 6760-6765.
45 A. D. Wang, L. Jiang, X. W. Li, Z. J. Xu, L. L. Huang, K. H. Zhang, X. Ji, and Y. F. Lu, Optics Exp., 2017, **25**(25), 31431-31442.
46 S. J. Henley, J. D. Carey, and S. R. P. Silva, *Phys. Rev. B.,* 2005, **72**, 195408.
47 Y. Y. Wu, N. Y. Dong, S. F. Fu, J. D. Fowlkes, L. Kondic, M. A. Vincenti, D. D. Ceglia, P. D. Rack, *ACS Appl. Mater. Interfaces,* 2014, **6**, 5835–5843.
48 P. D. Rack, Y. F. Guan, J. D. Fowlkes, A. V. Melechko, M. L. Simpson, *Appl. Phys. Lett.*, 2008**, 92**, 223108.
49 Y.Y. Wu, N. Y. Dong, S. F. Fu, J. D. Fowlkes, L. Kondic, M. A. Vincenti, D. Ceglia, and P. D. Rack, *ACS Appl. Mater. Interfaces,* 2014, **6**, 5835–5843.
50 P. D. Rack, Y. F. Guan, J. D. Fowlkes, A. V. Melechko, and M. L. Simpson, *Appl. Phys. Lett.,* 2008, **92**, 223108.
51 J. Wang, Y. T. Chen, X. Chen, J. M. Hao, M. Yan, M. Qiu, *Opt. Express,* 2011, **19** (15), 14726.
52 N. A. Roberts, J. D. Fowlkes, K. Mahady, S. Afkhami, L. Kondic, P. D. Rack, *ACS Appl. Mater. Interfaces,* 2013, **5**, 4450–4456.